The Journal of Chemical Physics ARTICLE pubs.aip.org/aip/jcp

Modeling ethanol/water adsorption in all-silica zeolites using the real adsorbed solution theory

Cite as: J. Chem. Phys. 162, 024703 (2025); doi: 10.1063/5.0230109
Submitted: 22 July 2024 • Accepted: 23 December 2024 •
Published Online: 9 January 2025

Anne V. Le,[1] Michael Tsapatsis,[2] J. Ilja Siepmann,[3] and Peng Bai[1,a)]

AFFILIATIONS

[1] Department of Chemical Engineering, University of Massachusetts Amherst, 686 North Pleasant Street, Amherst, Massachusetts 01003-9303, USA
[2] Department of Chemical and Biomolecular Engineering & Institute for NanoBioTechnology, Johns Hopkins University, Baltimore, Maryland 21218-2625, USA and Applied Physics Laboratory, Johns Hopkins University, Laurel, Maryland 20723, USA
[3] Department of Chemistry and Chemical Theory Center, University of Minnesota, Minneapolis, Minnesota 55455-0431, USA and Department of Chemical Engineering and Materials Science, University of Minnesota, Minneapolis, Minnesota 55455-0132, USA

Note: This paper is part of the JCP Special Topic on Monte Carlo Methods, 70 Years After Metropolis *et al.* (1953).
[a)]**Author to whom correspondence should be addressed:** pengbai@umass.edu

ABSTRACT

A comprehensive set of single-component and binary isotherms were collected for ethanol/water adsorption into the siliceous forms of 185 known zeolites using grand-canonical Monte Carlo simulations. Using these data, a systematic analysis of ideal/real adsorbed-solution theory (IAST/RAST) was conducted and activity coefficients were derived for ethanol/water mixtures adsorbed in different zeolites based on RAST. It was found that activity coefficients of ethanol are close to unity while activity coefficients of water are larger in most zeolites, indicating a positive excess free energy of the mixture. This observation can be attributed to water/ethanol interactions being less favorable than water/water interactions in the single-component adsorption of water at comparable loadings. The deviation from ideal behavior can be highly structure-dependent but no clear correlation with pore diameters was identified. Our analysis also demonstrates the following: (1) accurate unary isotherms in the low-loading regime are critical for obtaining physically sensible activity coefficients; (2) the global regression scheme to solve for activity model parameters performs better than fitting activity models to activity coefficients calculated locally at each binary state point; and (3) including the dependence on adsorption potential offers only a minor benefit for describing binary adsorption at the lowest fugacities. Finally, the Margules activity model was found incapable of capturing the non-ideal adsorption behavior over the entire range of fugacities and compositions in all zeolites, but for conditions typical of solution-phase adsorption, RAST predictions using zeolite-specific or even bulk Margules parameters provide an improved description compared to IAST.

I. INTRODUCTION

Adsorption isotherms are equilibrium relationships at constant temperature that connect the amount of adsorbed molecules on a sorbent material to the chemical potentials of the sorbate molecules, expressed as a function of either their pressure (in the case of single-component adsorption) or of the total pressure and compositions (in the case of multi-component adsorption).[1] The knowledge of adsorption isotherms in nanoporous materials, such as zeolites and metal-organic frameworks (MOFs), is key to the design of efficient adsorption- or membrane-based separation processes. However, acquiring mixture isotherms, either experimentally or computationally, can be time and resource intensive, as the number of data points required to fully characterize the adsorption equilibria increases exponentially with the number of components in the mixture. As a result, mixture adsorption is often predicted from single-component isotherms using models such as the adsorbed solution theory initially proposed by Myers and Prausnitz.[2]

In their treatment, the adsorbed phase is described using the framework of solution thermodynamics, but changes in the μ dn

term for the sorbent as a result of adsorption are expressed in terms of spreading pressure (i.e., due to the "spreading" of sorbate molecules on the sorbent surface), which is a new intensive variable introduced to define the state of the adsorbed phase. To make predictions of mixture loadings, an often-adopted practice is to further assume the adsorbed mixtures as ideal, leading to the ideal adsorbed solution theory (IAST). IAST is perhaps the most widely used mixture adsorption model, enjoying great successes for many important systems.[3] Due to its popularity, the accuracy of IAST has been the subject of constant scrutiny,[4–10] with significant deviations reported for mixtures that exhibit either preferential interactions with the sorbent or non-ideal interactions among the mixture components themselves. These deviations are not unexpected given the assumptions underlying IAST. Indeed, corrections have long appeared in the literature in the form of activity coefficients. Largely parallel to the development for non-confined liquid mixtures, various activity models have been used, including Margules,[11] Wilson,[12] NRTL,[13] Hildebrand,[14] and UNIQUAC.[15] The resulting model is usually referred to as the real adsorbed solution theory (RAST), which can describe mixture adsorption equilibria quantitatively and can be used for process design and optimization.[16]

While activity coefficients that quantify non-ideality have been broadly collected and tabulated for non-confining systems, they are essentially absent for adsorbed mixtures, as the exact non-ideal mixture behavior is sorbent-dependent. In this work, grand-canonical Monte Carlo (GCMC) simulations were used to calculate the unary and binary isotherms for the adsorption of ethanol and water into siliceous zeolites for all framework types cataloged by the International Zeolite Association (IZA).[17] Activity coefficients were analyzed using RAST and fitted to the Margules activity model. While we did not identify clear trends of activity coefficients with common structural descriptors, we hope this collection of isotherms provides a useful dataset for more sophisticated future analysis. In the following, we first briefly summarize the key equations of IAST/RAST, outline different analysis procedures, and discuss the treatment of the adsorption from a compressed liquid phase. We then illustrate the IAST/RAST analyses for a few representative zeolites before presenting the results for all zeolites.

II. METHODS

A. Ideal/real adsorbed solution theory

As a brief summary, IAST/RAST[2] introduces adsorption potential, Ψ, or equivalently, spreading pressure, π, as an intensive variable to characterize the adsorbed phase, which is obtained by integrating either mixture or unary adsorption isotherms, $N_{\mathrm{m}}(p_{\mathrm{m}})$ or $N_i(p_i)$, to the total pressure of the mixture, p_{t}, or some imagined pressure for the ith component, p_i^0 (in this section, we ignore the difference between fugacity and pressure in the vapor phase),

$$\Psi(p_i^0) = \frac{\pi A}{RT} = \int_0^{p_{\mathrm{t}}} \frac{N_{\mathrm{m}}(p_{\mathrm{m}})}{p_{\mathrm{m}}}\,\mathrm{d}p_{\mathrm{m}}, \tag{1}$$

$$= \int_0^{p_i^0} \frac{N_i(p_i)}{p_i}\,\mathrm{d}p_i, \quad i = 1 \ldots C, \tag{2}$$

where C is the number of components in the mixture, A is the (unknown) sorbent surface area, R is the gas constant, and T is temperature. IAST/RAST further derives a Raoult's law-type relationship,

$$p_i^0(\Psi) x_i \gamma_i = p_{\mathrm{t}} y_i, \quad i = 1 \ldots C, \tag{3}$$

where x_i is the adsorbed-phase molar fraction, γ_i is the adsorbed-phase activity coefficient, and y_i is the vapor-phase molar fraction.

When using IAST to predict mixture adsorption from single-component isotherms, γ_i is assumed to be unity, $N_i(p_i)$ is known, while $N_{\mathrm{m}}(p_{\mathrm{m}})$ is not available. One specifies as input p_{t} and y_i and solves for $p_i^0(\Psi)$ and the adsorbed-phase composition x_i (e.g., three unknowns for a binary mixture: p_1^0, p_2^0, and x_1) using the above-mentioned three independent equations [Eq. (2) gives a single equation: $\Psi(p_1^0) = \Psi(p_2^0)$, while Eq. (3) gives two; see the supplementary material for the definition of the objective function] following which the mixture loading, N_{m}, is found through the molar surface area of mixing,

$$\frac{1}{N_{\mathrm{m}}} = \sum_i \frac{x_i}{N_i(p_i^0)} + \sum_i x_i \frac{\partial \ln \gamma_i}{\partial \Psi} \overset{\mathrm{IAST}}{=} \sum_i \frac{x_i}{N_i(p_i^0)}, \tag{4}$$

$$N_i = N_{\mathrm{m}} \cdot x_i, \quad i = 1 \ldots C. \tag{5}$$

B. Activity models

When using RAST to predict mixture adsorption, an activity model (with $M + 1$ parameters) is further supplied to Eq. (3),

$$\begin{aligned} \ln \gamma_i &= f(T, \Psi, x_1, x_2, \ldots, x_{C-1}; A_1, A_2, \ldots, A_M, \zeta) \\ &= f'(T, x_1, x_2, \ldots, x_{C-1}; A_1, A_2, \ldots, A_M)[1 - \exp(-\zeta\Psi)], \end{aligned} \tag{6}$$

where A_j and ζ are model parameters. In this operation mode, there are $3C - 1$ independent equations [C of Eq. (3), $C - 1$ of Eq. (2), and C of Eq. (6)], which are used to solve for $3C - 1$ unknown variables (C of p_i^0, $C - 1$ of x_i, and C of γ_i).

Activity models developed for liquid mixtures are typically only a function of T and x_i, as liquid properties depend weakly on external pressure p. For adsorbed phases, however, p is replaced by π or Ψ and γ_i in general depend on Ψ. That is, an adsorbed equal-molar mixture will behave like an ideal solution at infinite dilution but may deviate significantly from ideality at saturation; an analogous limit of $p \to 0$ for bulk fluids similarly implies ideal gas mixtures. Following Myers *et al.*,[11,18] Eq. (6) imposes the dependence of γ_i on Ψ. If the Margules activity model is used, then

$$\begin{aligned} \ln \gamma_1 &= [A_{12} + 2(A_{21} - A_{12})x_1]x_2^2 \cdot [1 - \exp(-\zeta\Psi)], \\ \ln \gamma_2 &= [A_{21} + 2(A_{12} - A_{21})x_2]x_1^2 \cdot [1 - \exp(-\zeta\Psi)], \end{aligned} \tag{7}$$

and Eq. (4) regarding the excess surface area of mixing will read

$$\frac{1}{N_{\mathrm{m}}} = \frac{x_1}{N_1(p_1^0)} + \frac{x_2}{N_2(p_2^0)} + \zeta \exp(-\zeta\Psi) x_1 x_2 (A_{21} x_1 + A_{12} x_2). \tag{8}$$

This additional factor is sometimes ignored,[13,16] especially when using RAST to correlate binary adsorption data measured at a constant external pressure, as the available data often do not allow unambiguous determination of the Ψ dependence (see Sec. III).

Conversely, when mixture adsorption data are available (i.e., N_i, $N_m = \sum_i N_i$, and $x_i = N_i/N_m$ are known), activity coefficients γ_i can be empirically determined through several different routes.

1. In the local scheme, γ_i is determined at each mixture data point and fitted to Eq. (6). First, Ψ is calculated from the binary isotherm for a fixed-composition mixture with Eq. (1), after which p_i^0 is solved using Eq. (2). Finally, γ_i can be calculated using Eq. (3). It should be noted that Eq. (1) is derived by integrating the Gibbs adsorption isotherm (effectively a Gibbs–Duhem relationship),[1,19]

$$d\Psi = d\left(\frac{\pi A}{RT}\right) = \sum_i N_i \, d\ln p_i = \sum_i (N_m x_i) \, d\ln(p_t y_i)$$
$$= N_m \, d\ln p_t + \sum_i N_m x_i \, d\ln y_i$$

along a fixed-composition path, where $d\ln y_i = 0$ and thus the second term drops out. Alternatively, Ψ at each mixture data point can also be integrated first along a single-component path (i.e., $y_i = 1$) from $p_t = 0$ to the value of p_t in the mixture and then along a fixed-pressure path from $y_i = 1$ to y_i in the mixture,

$$\Psi = \frac{\pi A}{RT} = \int_0^{p_t} N_i \, d\ln p_i + \int_1^{y_i} N_m x_i \, d\ln y_i + \sum_{j\neq i} \int_0^{y_j} N_m x_j \, d\ln y_j.$$

2. In a global scheme, the activity model parameters are fitted to all available mixture data: if we have L mixture data points, Eqs. (2) and (3) [with Eq. (6) substituted in], and 8 define $2CL$ independent equations, which can be regressed to determine the $CL + M + 1$ unknown variables: p_i^0 at each of the L data points, activity model parameters A_j's, and ζ.
3. In another global scheme,[11] the only unknown variables are the $M + 1$ activity model parameters. Given an initial guess for $A_1, A_2, \ldots, A_M$ and ζ, γ_i can be computed from Eq. (6). Inverting $\Psi(p_i^0)$ gives $p_i^0(\Psi)$, which can be substituted into Eq. (8) to solve for Ψ. Based on $p_i^0(\Psi)$, x_i, and γ_i, Eq. (3) gives an independent prediction of $p_t y_i$, which can be compared to the actual mixture data to allow for the optimization of A_j's and ζ. Even though this regression scheme has a relatively small, fixed problem size compared to Scheme 2, the need to solve the nonlinear Eq. (8) makes it slower than Scheme 2 based on our observations.

To perform the numerical calculations, $N_m(p_m)$ and $N_i(p_i)$ were fitted to either piecewise linear functions or dual-site Langmuir models. $\Psi(p_i^0)$ has explicit expressions in both cases, while $p_i^0(\Psi)$ has explicit solutions for the piecewise linear fits but must be solved iteratively for the dual-site Langmuir fits. The regressions were performed using least squares of the relative errors; see the supplementary material for the definitions of the objective functions.

C. Adsorption of compressed liquids

Since the development by Myers and Prausnitz,[2] the majority of applications of IAST/RAST models have focused on gas-phase adsorption,[1,20] where there is no ambiguity regarding the pressure terms in Eqs. (2) and (3). In fact, Eq. (3) is derived by equating the chemical potential of the adsorbed mixture with that of a coexisting vapor phase,[1]

$$\mu_{ads,i}(T, \Psi, x_1, x_2, \ldots, x_{C-1}) = \mu_{vap,i}(T, p, y_1, y_2, \ldots, y_{C-1}), \quad (9)$$

$$\mu^0_{ads,i}(T, \Psi) + RT \ln(\gamma_i x_i) = \mu^0_{vap,i}(T) + RT \ln(p y_i), \quad (10)$$

where $\mu^0_{ads,i}(T, \Psi)$ represents the chemical potential of the ith component in its pure adsorbed state at the same adsorption potential Ψ. Considering the single-component adsorption equilibrium, an analogous equality of chemical potentials can be written,

$$\mu^0_{ads,i}(T, \Psi) = \mu_{vap,i}(T, p_i^0) = \mu^0_{vap,i}(T) + RT \ln(p_i^0), \quad (11)$$

where p_i^0 is the vapor pressure at which the unary adsorption potential equals Ψ. Substituting Eq. (11) into Eq. (10) gives Eq. (3).

The adsorption from a compressed liquid phase, however, presents interesting difficulties, as is the case with water adsorption into hydrophobic zeolites. Although representing single-component isotherms of compressed liquids using the total liquid pressure formally works,[21] it leads to large errors in Eq. (11) [i.e., p_{liq} is much larger than p_{vap}; see Eq. (12) below]. However, since the total pressure is above the saturation vapor pressure, liquid phase is the only stable bulk phase, which was represented explicitly in our previous GEMC simulations.[21] In this case, a more appropriate treatment is to use the pressure of a hypothetical vapor phase that has the same chemical potential as the compressed liquid. Roughly speaking, one can imagine starting from a single-component system of coexisting liquid and vapor phases and adding a second, insoluble gas component into the vapor region to raise the total pressure of the system, p_{liq}, the partial vapor pressure of the first component, p_{vap}, will increase as a result. To calculate p_{vap}, we integrate from the saturation vapor pressure p_{sat},[22]

$$\begin{gathered}
\mu_{liq}(T, p_{liq}) = \mu_{vap}(T, p_{vap}), \\
\cancel{\mu_{liq}(T, p_{sat})} + \int_{p_{sat}}^{p_{liq}} \left(\frac{\partial \mu}{\partial p}\right)_{liq} dp = \cancel{\mu_{vap}(T, p_{sat})} + \int_{p_{sat}}^{p_{vap}} \left(\frac{\partial \mu}{\partial p}\right)_{vap} dp, \\
\int_{p_{sat}}^{p_{liq}} \widetilde{V}_{liq} \, dp = \int_{p_{sat}}^{p_{vap}} \widetilde{V}_{vap} \, dp, \\
\widetilde{V}_{liq}(p_{liq} - p_{sat}) = \int_{p_{sat}}^{p_{vap}} \frac{RT}{p} \, dp = RT \ln \frac{p_{vap}}{p_{sat}}, \\
p_{vap} = p_{sat} \exp\left[\frac{\widetilde{V}_{liq}(p_{liq} - p_{sat})}{RT}\right],
\end{gathered} \quad (12)$$

where the vapor phase is assumed to be ideal and the liquid molar volume $\widetilde{V}_{liq}$ is assumed to be pressure-independent. It should be noted that this complication does not appear in GCMC simulations, in which one can vary the fugacity f continuously from the vapor state to the compressed liquid state and calculate the corresponding values of μ. In GEMC simulations where the vapor pressure of a compressed liquid may not be known, Eq. (12) can be used for the conversion.

D. Computational details

For IAST/RAST analyses, three datasets of adsorption per zeolite structure are needed, which are the adsorption isotherms for water, ethanol, and their binary mixtures. GCMC simulations were used to obtain these isotherms at $T = 323$ K. For single-component adsorption, chemical potentials were calculated from fugacities: $\mu_i = \mu_{\text{intra,i}} + k_B T \ln f_i$, where $\mu_{\text{intra,i}}$ are intramolecular contributions calculated for an isolated molecule of type i.[23] For binary adsorption, two campaigns were conducted. In Campaign A, solution-phase adsorption was simulated from liquid mixtures under an external pressure of $p_{\text{ext}} = 1.013\,25 \times 10^5$ Pa. μ was calculated from f, which is taken to be the partial pressures at different solution-phase compositions from previous Gibbs-ensemble Monte Carlo (GEMC) simulations.[21] In Campaign B, a two-dimensional survey was performed with $f_{\text{total}} = f_{\text{H2O}} + f_{\text{EtOH}}$ ranging from 9×10^1 to 5×10^5 Pa roughly uniformly spaced logarithmically and at each total fugacity, $y_{\text{EtOH}} = 0.1, 0.3, 0.5, 0.7$, and 0.9. All zeolites deposited in IZA's online database[17] were considered except for structures with pore-limiting diameters (PLD) less than 4 Å. Here, PLDs were calculated using Zeo++[24] and the cutoff value was determined based on 4A zeolites as it is used for membrane separation that excludes ethanol. Zeolites DDR[25] and CHA[26] (both have PLD = 3.55 Å and DDR shows an oval-shaped pore opening) were added back to allow comparisons with the work of Krishna and van Baten,[8,9] resulting in a total of 185 zeolites.

To sample the configurational phase space, four types of Monte Carlo (MC) moves were used with about 20% assigned to center-of-mass translations, 20% rigid-body rotations, 10% configurational-biased MC (CBMC) regrowths,[27–30] and 50% insertion/deletion moves. In mixture simulations, all MC moves were performed with equal probabilities on water and ethanol molecules except for CBMC moves that were only done on ethanol. The sorbate–sorbate and sorbate–zeolite interactions were described by the TIP4P,[31] TraPPE-UA,[32] and TraPPE-zeo[33] force fields. Zeolites were treated as rigid during the simulations by fixing framework atoms at their crystallographic coordinates. Consequently, sorbate–zeolite interactions depend only on the sorbate configuration and were, therefore, pretabulated. Inaccessible regions (e.g., sodalite cages in zeolite FAU) were not blocked, as ethanol and water do not enter these regions at loadings relevant for the binary adsorption and the RAST analysis. Lennard-Jones interactions were evaluated to a spherical cutoff of $r_{\text{cut}} = 14$ Å with analytical tail corrections, while Coulomb interactions were calculated using the Ewald summation technique using a convergence parameter, $\kappa = 3.2/r_{\text{cut}}$, which gives a reciprocal-space cutoff of 1.44 Å^{-1}.[23] The choice of force fields used for adsorbates and adsorbent has been extensively validated in prior work and was found to reproduce experimental measurements on high-quality, all-silica zeolites (e.g., water adsorption in MFI,[21,33] ethanol adsorption in MFI,[21,33] and ethanol/water adsorption in MFI[34] and FER[35]). They have also been used for fluid phase equilibria and vapor-to-liquid nucleation studies.[36] To assess equilibration, simulations were run in iterations of 10^6 steps each. Changes in loadings were checked after each run if they fall below 5% of the respective loadings for binary simulations or of the total loadings for unary simulations. In all cases, the threshold is kept above at least one molecule in the simulation box. Following this protocol, most state points needed 1–5 equilibration stages, after which production stages were run for 4×10^6 steps. Six independent simulations were used for unary water isotherms due to the phase-transition-like steep uptake in loading.

As discussed in the supplementary material, eight independent simulations were performed for equimolar mixtures in MFI and DDR to assess the adequacy of the simulation length (see Figs. S1 and S2). We did not find significant changes in RAST analysis in terms of prediction quality for isotherm loadings and selectivity using longer trajectories. In addition, we observed that for the adsorption of ethanol/water mixtures in hydrophobic all-silica zeolites, the standard Herington test cannot be easily applied due to the following: (a) x_{EtOH} often does not cover the entire composition range and (b) $\int_{x_1=0}^{x_1=1} \tilde{A}^E/RT(\partial\pi/\partial x_1)_{T,p}\, dx_1$ is not small and cannot be ignored (see Fig. S3).

III. RESULTS AND DISCUSSION

A. IAST predictions involving compressed liquids

Figure 1(a) compares IAST predictions obtained by expressing the adsorption isotherm of water as a function of the pressure of a coexisting vapor phase or of the total pressure exerted over the compressed liquid (see Sec. II C). In both cases, the amount of adsorbed ethanol is well reproduced, with values of Q_{EtOH} predicted using external pressure slightly higher than those using vapor pressure when $f_{\text{EtOH}} > 10^3$ Pa and slightly lower when $f_{\text{EtOH}} < 10^3$ Pa. On the other hand, distinctly different predictions are found for the amount of adsorbed water. Using external pressure, IAST significantly underestimates water loading due to the exceedingly high fugacity, f^0_{H2O}, required to achieve the same spreading pressure as

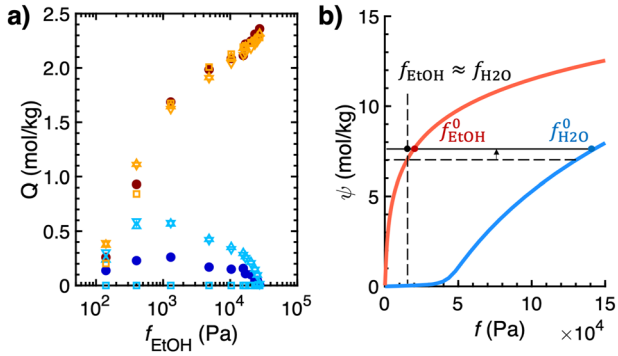

FIG. 1. (a) Adsorption isotherms for solution-phase adsorption in zeolite MFI at $T = 323$ K and $p = 1.013\,25 \times 10^5$ Pa, showing amounts of adsorption for ethanol (red) and water (blue) as a function of f_{EtOH} from GCMC simulations in Campaign A (filled circles) and IAST predictions (up triangles). For comparison, IAST predictions using single-component isotherms from previous GEMC simulations[21] are also shown using the vapor pressure converted via Eq. (12) (down triangles) and using the external pressure over the compressed liquid (squares). Other than the last case, all other IAST analyses use the pressure of a coexisting vapor phase for the adsorption of compressed liquid water. (b) Illustration of the IAST solution process for the adsorption of an equal-molar gas mixture with fugacities indicated by the vertical dashed line. On a plot of adsorption potential vs fugacity, the horizontal lines ensure the condition of equal Ψ. The horizontal dashed line represents an initial guess, where $f^0_{\text{EtOH}} = f_{\text{EtOH}}$. This line is moved upward iteratively until it finds a vertical position (solid black line) that satisfies $x_{\text{EtOH}} + x_{\text{H2O}} = f_{\text{EtOH}}/f^0_{\text{EtOH}} + f_{\text{H2O}}/f^0_{\text{H2O}} = 1$.

ethanol [Eq. (2)], which in turn leads to very small molar fraction x_{H2O} as demanded by Eq. (3). If vapor pressure is used, IAST would instead overestimate water loading. Finally, the IAST results based on the unary water isotherm computed previously using GEMC simulations[21] agree very well with the results based on the new unary water isotherm obtained in this work using GCMC simulations, when the appropriate vapor pressure is calculated from the external pressure according to Eq. (12), indicating the accuracy of the conversion.

To better understand the opposite trends of IAST predictions, Fig. 1(b) shows the IAST solution process for the sixth lowest ethanol concentration, which has $f_{EtOH} = 1.5655 \times 10^4$ Pa and $f_{H2O} = 1.6664 \times 10^4$ Pa; i.e., the aqueous mixture corresponds roughly to an equal-molar gas mixture. The IAST solution is represented by the solid black line, which is horizontal due to the condition of equal Ψ. Imagine an initial guess indicated by the horizontal dashed line, for which $f_{EtOH}/f^0_{EtOH} + f_{H2O}/f^0_{H2O} = 1 + f_{H2O}/f^0_{H2O} > 1$. The dashed line must be moved upward to a vertical position that satisfies $f_{EtOH}/f^0_{EtOH} + f_{H2O}/f^0_{H2O} = 1$. When using external pressure, the blue curve representing Ψ_{H2O} is shifted substantially to the right (i.e., to much higher fugacities). The initial guess needs to slide upward only slightly since $x_{EtOH} = f_{EtOH}/f^0_{EtOH} \approx 1$ and $x_{H2O} = f_{H2O}/f^0_{H2O} \approx 0$ are immediately satisfied. When using vapor pressure, x_{H2O} is much larger, but whether these larger values of x_{H2O} lead to under- or over-predictions compared to mixture simulations depends on the balance of the dominant interactions of water in its unary adsorption vs those in binary adsorption. Even though the TraPPE-zeo force field used in this work did not include water adsorption in its training data,[33] it was found to reproduce the hydrophobic nature very well compared to the experimental measurements on defect-free, all-silica MFI zeolites.[37] As a result, significant uptake of water is driven mostly by strong sorbate–sorbate interactions due to hydrogen bonding, and the degree of hydrogen bonding is diminished when ethanol is co-adsorbed,[38] suggesting a positive excess free energy and $\gamma_{H2O} > 1$ (see below for further discussions). We note that an enhanced co-adsorption of water was reported for zeolite DDR recently by Krishna and van Baten (cf., Fig. 13 of Ref. 8), which we speculate is due to the different partial charges in the force fields on zeolite framework atoms, $q_O = -1.025$ in that work[8,39] vs $q_O = -0.75$ used here.

B. Activity coefficients

Figures 2 and S4 show the activity coefficients and associated Margules activity models derived according to the different schemes of RAST analysis discussed in Sec. II B. Activity coefficients represented by the filled symbols for each binary state point were calculated according to Scheme 1. The collection of activity coefficients across all combinations of fugacity and gas-phase composition from both Campaign A and Campaign B were then fitted to the Margules equation. As discussed in Sec. II B, activity models for the adsorbed phase should, in principle, depend on the adsorption potential, and the Margules equation for bulk liquid mixtures should be modified to enforce ideality as Ψ approaches zero, as done in Eq. (7). The importance of the correction factor, $1 - \exp(-\zeta\Psi)$, has been examined carefully by Krishna and van Baten.[6,7,9,10] However, including this additional factor was found here to be nearly indistinguishable from ignoring it (i.e., comparing dashed and dotted lines) in many zeolites. An alternative way of deriving the activity model is by fitting the Margules parameters directly according to Scheme 2 without calculating activity coefficients first. The effect of including the Ψ dependence was found similarly negligible for MFI and DDR in this global regression scheme (i.e., comparing solid and dashed–dotted lines). The lack of Ψ-dependence is either because the optimized ζ value is too large (see the numerical results for MFI and DDR presented in Table S1) or because the other Margules parameters, A_{12} and A_{21}, may adapt to achieve fits of similar quality. We note that simply removing the Ψ term

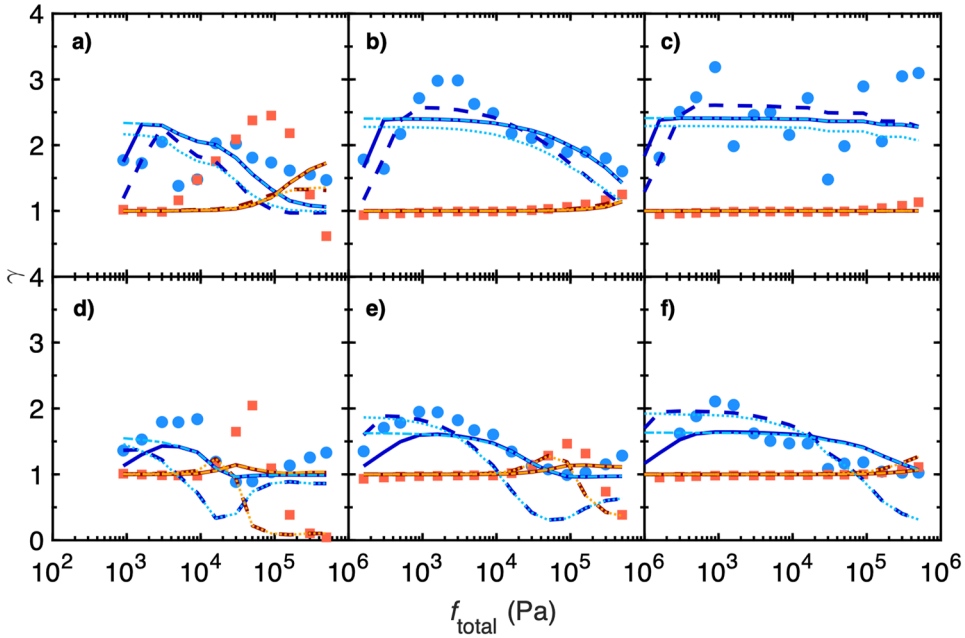

FIG. 2. RAST activity coefficients as a function of total fugacity for binary adsorption of ethanol (red) and water (blue) in MFI [(a)–(c)] and DDR [(d)–(f)] at $T = 323$ K and gas-phase composition y_{EtOH} = [(a)/(d)] 0.1, [(b)/(e)] 0.5, and [(c)/(f)] 0.9. γ calculated algebraically using Scheme 1 of Sec. II B are represented by the filled symbols. The dotted and dashed lines represent regression of γ across all state points to the Margules equation without and with Ψ-dependence, respectively. The dashed–dotted and solid lines represent the Margules model determined according to Scheme 2 without and with Ψ-dependence, respectively.

without reoptimizing other Margules parameters would certainly lead to larger differences, as demonstrated in Fig. 4 of Ref. 9. Krishna and van Baten have shown that if the unary isotherms can be modeled by multi-site Langmuir isotherms, the correction factor represents the fractional occupancy and ζ is essentially the inverse saturation loading: $1/N_{m,sat} = x_1/N_{1,sat} + x_2/N_{1,sat}$.[9,10] However, since the unary water isotherms are not described well by multi-site Langmuir isotherms in many zeolites and the mixture saturation loading, $N_{m,sat}$, is dependent on the adsorbed-phase composition, it is hard to use this result to directly obtain a single value of ζ. To test the effect of using more realistic values according to $1/N_{m,sat}$, Fig. S5 shows RAST predictions by constraining $\zeta < 1$. The objective function (see the definition of $\epsilon_{prediction}$ in Sec. S1) is 23 times larger (worse) when constrained ($\zeta = 0.41$) than unconstrained ($\zeta = 40.1$). We, therefore, treated ζ as a fitting parameter, as done in most prior studies.

Both the local and global schemes yield essentially identical results for ethanol, which clusters around $\gamma_{EtOH} = 1$ in most cases. By contrast, γ_{H2O} is much noisier due to error propagation, and the two schemes generate rather different predictions. γ_{H2O} values from the global scheme appear to have weaker variations and are overall smaller in magnitude, but both are greater than unity for almost all state points. γ_{H2O} lies roughly between 1.5 and 3 in MFI when $y_{EtOH} = 0.5$ and 0.9, but is largely less than 2 in DDR and in MFI when $y_{EtOH} = 0.1$. For some zeolites such as DDR, the binary data across the entire range of total fugacities and compositions (see Figs. 2 and S4) are not described well by the best-fit Margules equation from either scheme. The calculation of activity coefficients relies on equating the adsorption potential for binary and unary adsorption, but unlike other intensive variables such as pressure, Ψ cannot be measured directly but must be integrated from the isotherms from $p \to 0$ [Eqs. (1) and (2)]. As a consequence, obtaining physically sensible values of γ depends on the quality of the isotherms in the low-pressure regime.[15] As shown in Fig. 3, at all gas-phase compositions, the low-pressure portion of the binary isotherms (black diamonds) in both MFI and DDR are primarily due to ethanol adsorption (red squares). This leads to $x_{EtOH} \approx 1$ and nearly identical adsorption potentials at low pressures (see Fig. 4) for binary adsorption (black solid lines) and for unary ethanol adsorption (red solid lines), which in turn means $f^0_{EtOH} \approx f_t y_{EtOH}$ in Eq. (3) and thus $\gamma_{EtOH} \to 1$ under these conditions.

To test the effect of mismatched low-pressure isotherms, Figs. 3 and 4 also include the scenario when additional binary data points are added at even lower fugacities ($f_{EtOH} < 80$ Pa), which can correspond to solution-phase adsorption with a dilute solute. The resulting black dotted lines for Ψ_m now deviate from the red solid lines representing Ψ_{EtOH}. As a result, γ_{EtOH} does not approach unity even at the limits of $\Psi \to 0$ and $x_{EtOH} \to 1$ (cf., open squares in Fig. S6). One may rightfully argue that the failure to obtain physically sensible activity coefficients arises from the fact that piecewise linear fits of the isotherm with respect to the logarithm of fugacity, $Q = k \ln f$, cannot reproduce the correct asymptotic behavior in the Henry's law regime, which requires $Q = kf$. However, such failures are not always easily remedied by, for example, using an isotherm model that does have the correct low-pressure limit such as the dual-site Langmuir model

$$\hat{Q}(f) = \frac{Q_{max,1} K_1 f}{1 + K_1 f} + \frac{Q_{max,2} K_2 f}{1 + K_2 f} \tag{13}$$

where $Q_{max,i}$ and K_i are model parameters. The red dashed lines in Fig. 3 show the dual-site Langmuir model fitted to the unary ethanol

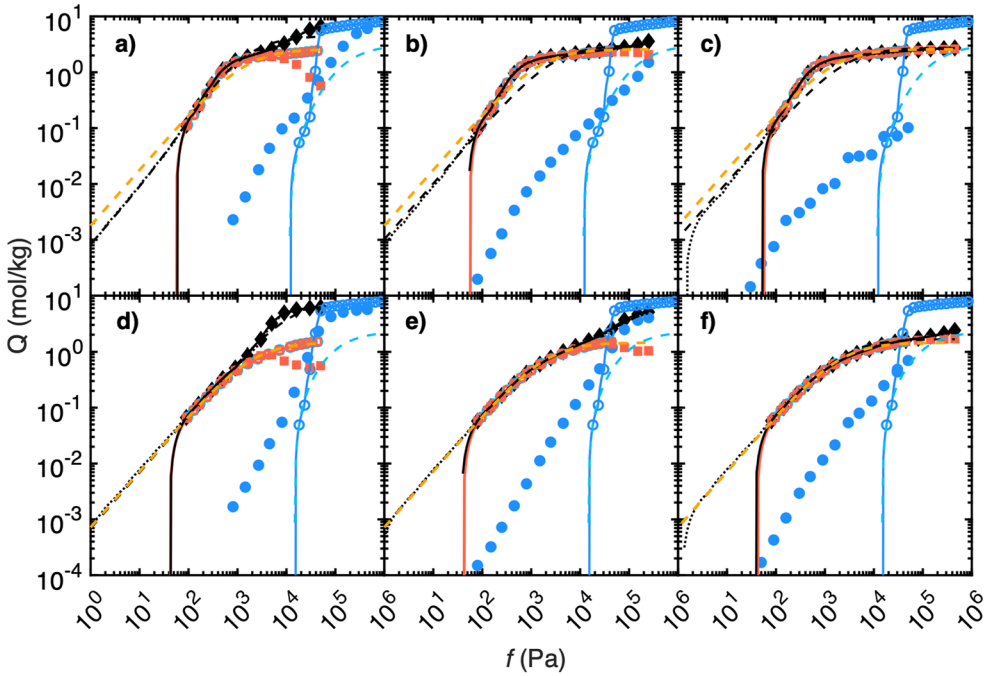

FIG. 3. Adsorption isotherms for ethanol (red squares) and water (blue circles) in MFI [(a)–(c)] and DDR [(d)–(f)] at $T = 323$ K and gas-phase composition y_{EtOH} = [(a)/(d)] 0.1, [(b)/(e)] 0.5, and [(c)/(f)] 0.9. Total loadings of the adsorbed mixture ($Q_m = Q_{EtOH} + Q_{H2O}$) are represented by the filled black diamonds. Component loadings from the unary and binary isotherms are represented by the empty and filled symbols, respectively. Q_{EtOH} and Q_m are shown as a function of f_{EtOH} while Q_{H2O} is shown as a function of f_{H2O}. Piecewise linear fits of each isotherm are represented by the solid lines, which start at the fugacity where the fitted lines cross zero. For comparison, dual-site Langmuir fits are represented by the dashed lines. The black dotted lines represent the piecewise linear fits when additional binary data points are added at lower pressures ($f_{EtOH} < 80$ Pa).

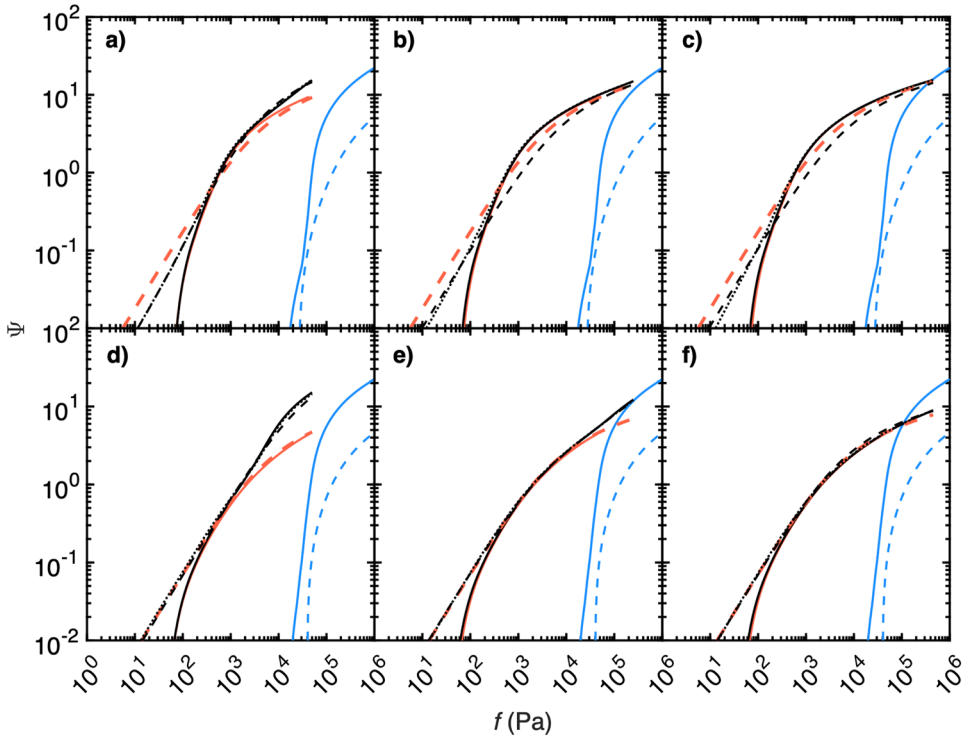

FIG. 4. Adsorption potential in MFI [(a)–(c)] and DDR [(d)–(f)] at T = 323 K and gas-phase composition y_{EtOH} = [(a)/(d)] 0.1, [(b)/(e)] 0.5, and [(c)/(f)] 0.9. The solid lines of different colors correspond to unary ethanol (Ψ_{EtOH}, red), unary water (Ψ_{H2O}, blue), and their binary mixture (Ψ_m, black). Ψ_{EtOH} and Ψ_m are shown as a function of f_{EtOH}, while Ψ_{H2O} is shown as a function of f_{H2O}. For comparison, the dashed or dotted lines show the adsorption potential from integrating the corresponding isotherms shown in Fig. 3.

isotherms by minimizing the least-squared error in relative loadings, which agree very well with the binary isotherms in the case of DDR but less so with MFI. Therefore they do not fully remove the errors in γ_{EtOH} (see red triangles for MFI in Fig. S6). These comparisons suggest that to obtain accurate activity coefficients, the unary isotherms for each mixture component, or their fitted versions, must yield accurate adsorption potentials at least for the regimes above the minimum adsorption potential for the mixture. Extending the

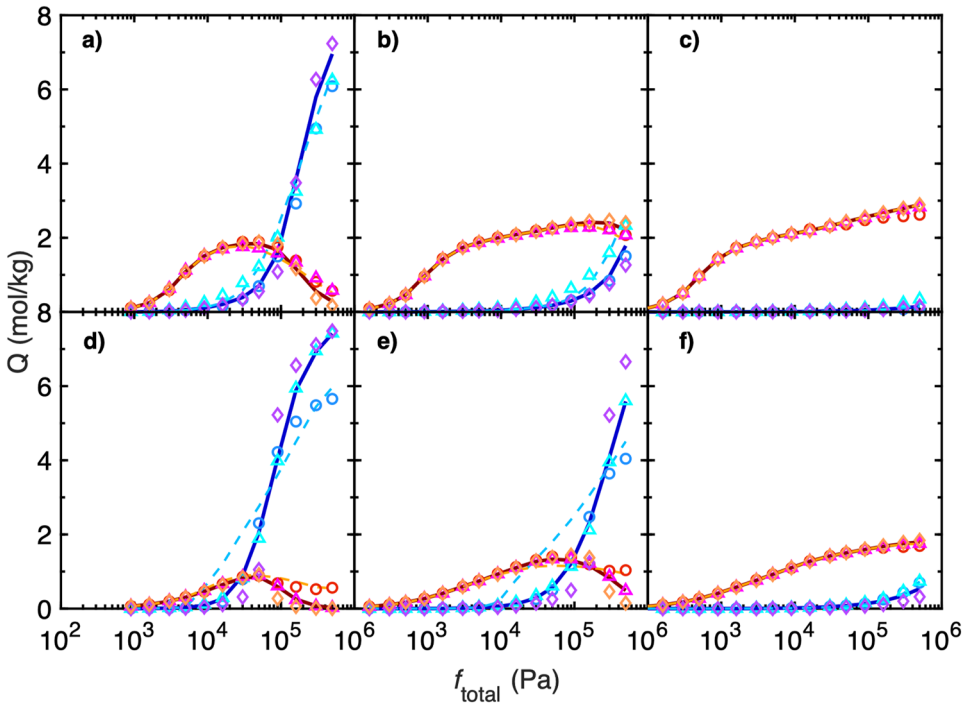

FIG. 5. Binary adsorption isotherms in MFI [(a)–(c)] and DDR [(d)–(f)], showing amounts of adsorption for ethanol (red) and water (blue) as a function of f_{total} from GCMC simulations in Campaign B (open circles) at T = 323 K and gas-phase composition y_{EtOH} = [(a)/(d)] 0.1, [(b)/(e)] 0.5, and [(c)/(f)] 0.9. RAST predictions using Schemes 1 and 2 are shown as dashed and solid lines, respectively. For comparison, RAST predictions using bulk Margules coefficients for ethanol (orange) and water (purple) are shown as diamonds, and IAST predictions for ethanol (magenta) and water (cyan) are shown as up triangles.

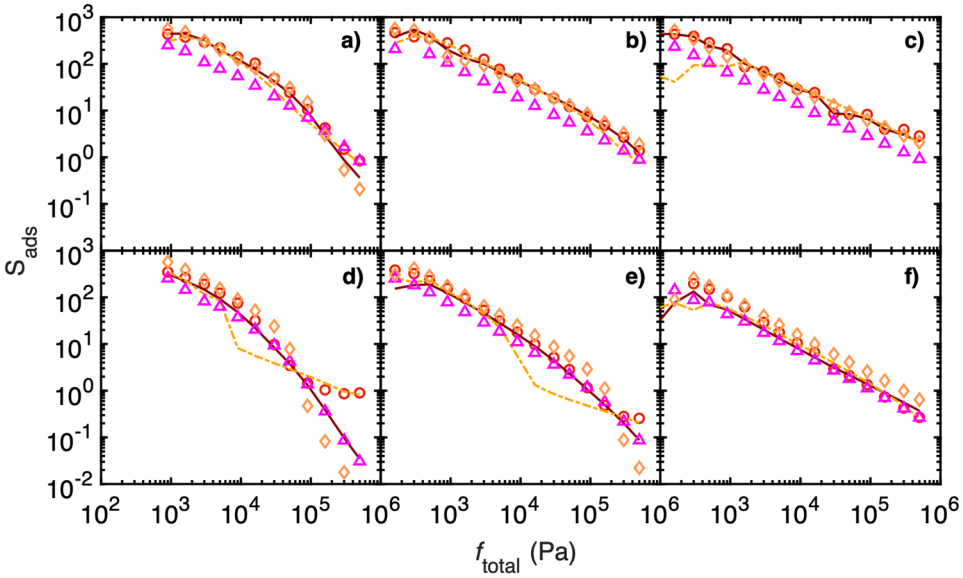

FIG. 6. Ethanol/water selectivity as a function of f_{total} in MFI [(a)–(c)] and DDR [(d)–(f)] from GCMC simulations in Campaign B (red circles) at T = 323 K and gas-phase composition y_{EtOH} = [(a)/(d)] 0.1, [(b)/(e)] 0.5, and [(c)/(f)] 0.9. RAST predictions using Schemes 1 and 2 are shown as dashed and solid lines, respectively. For comparison, RAST predictions using bulk Margules coefficients and IAST predictions are shown as orange diamonds and magenta up triangles, respectively.

unary isotherms to even lower fugacities has minimal influence on RAST predictions (see Sec. S5, Figs. S7–S11). Experimentally, it may be difficult to reach the Henry's law regime for all mixture components. To deal with this challenge, Gamba *et al.* proposed an alternative solution by rewriting Eqs. (1) and (2) relative to a low-pressure reference data point and treating it as an additional fitting parameter.[15]

C. RAST predictions of binary adsorption

It is worth noting that the scatter in γ_{H2O} does not arise from large uncertainties in the adsorption isotherms, which are shown as open symbols in Fig. 5. It is therefore interesting to ask how much deviations in activity coefficients can be tolerated before there are discernible differences in RAST predictions. To answer this question, Fig. 5 compares RAST-predicted isotherms for MFI and DDR using Margules activity models determined with the two different regression schemes, using the Margules model for bulk ethanol/water mixtures, and assuming $\gamma = 1$ (IAST). Overall, Scheme 2 gives better agreement, with a mean-squared error (MSE) of 0.0227 and 0.136 for MFI and DDR, respectively, which are about 1–2 orders of magnitude better than the MSE from Scheme 1 (MSEs are relative errors; see definitions of $\epsilon_{prediction}$ in Sec. S1). The most significant prediction error with Scheme 2 is observed where the fugacity of water, f_{H2O}, is high and water loading exceeds ethanol loading. In this reversal regime, RAST underpredicts ethanol loadings and overpredicts water loadings, which can be traced primarily to the poor agreement of Margules activity coefficients for ethanol: For the 1:9 ethanol/water mixture, as f_{total} increases from 2×10^4 to 5×10^5 Pa, Margules activity coefficients fitted via Scheme 2 increase slightly from 1 to 1.7 in MFI and stay within 1–1.2 in DDR, while simulation-derived γ_{EtOH} first increases before a rapid decrease to nearly zero. In other words, ethanol molecules experience more favorable interactions when they are surrounded by water molecules than when they are surrounded by other ethanol molecules.

By contrast, Margules activity coefficients fitted via Scheme 1 result in better agreement in the reversal regime at the expense of more significant overprediction of water loading at lower fugacities of water. These differences can be seen more clearly in the log-log plots of selectivity vs fugacity (Fig. 6), where the selectivity is defined as $S = (x_{EtOH}/x_{H2O})/(y_{EtOH}/y_{H2O})$. The RAST-predicted selectivity for ethanol over water using Scheme 2 Margules activity

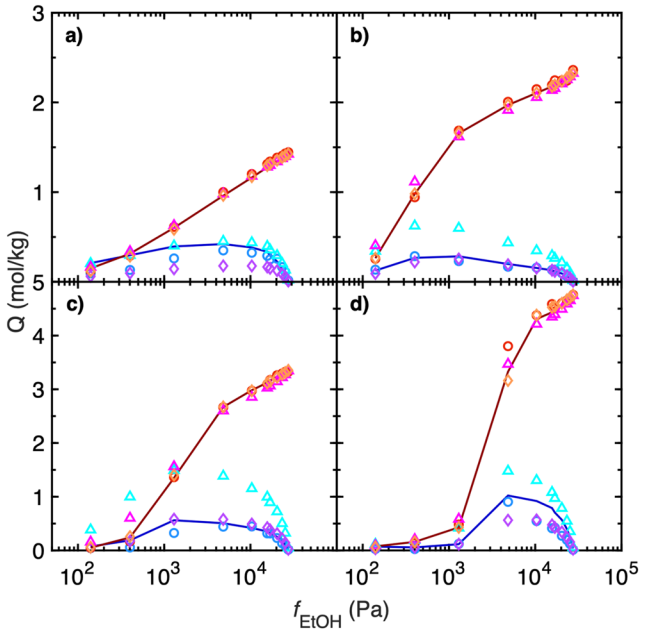

FIG. 7. Adsorption isotherms for solution-phase adsorption at T = 323 K and p = 1.013 25 × 10^5 Pa, showing amounts of adsorption for ethanol (red) and water (blue) as a function of f_{EtOH} from GCMC simulations in Campaign A (open circles) for (a) DDR, (b) MFI, (c) BEA, and (d) LTA. RAST predictions using Scheme 2 are shown as solid lines, RAST predictions using bulk Margules coefficients for ethanol (orange) and water (purple) are shown as diamonds, and IAST predictions for ethanol (magenta) and water (cyan) are shown as up triangles.

model agrees very well at most state points except in the reversal regime, where it underpredicts by about one and two orders of magnitude in MFI and DDR, respectively, at $f_{total} = 5 \times 10^5$ Pa and $y_{EtOH} = 0.1$. On the other hand, Scheme 1 Margules model gives much better predictions in this regime, but gives selectivities in the normal regime that are smaller by almost an order of magnitude at a number of state points. As discussed in Sec. IV, the reversal regime is more of a theoretical interest that will only be encountered under extreme external pressures.

Interestingly, using Margules parameters for bulk ethanol/water mixtures gives surprisingly good predictions of both ethanol and water loadings in MFI. It somewhat underpredicts water loadings in the normal, ethanol-selective regime in DDR. In the reversal regime, the bulk Margules model similarly overpredicts water loading and underpredicts ethanol loading in both MFI and DDR. In CHA, RAST predictions of loadings and selectivity using bulk Margules parameters are on par with those based on Scheme 2 (Fig. S12). This is in contrast to the observations by Krishna and van Baten for CHA,[9] where they found that both γ_{H2O} and γ_{EtOH} are smaller than one (page S98) and can therefore not be described well by the bulk Margules parameters. Again, we suspect that the different trends are due to the choice of force fields, elaborated at the end of Sec. III A.

As discussed in Sec. III A, IAST predictions of water loadings are higher than loadings from the mixture simulations in MFI, leading to a smaller selectivity for ethanol by roughly a factor of two. In DDR, however, IAST predictions are nearly indistinguishable from the RAST predictions using Scheme 2 Margules activity coefficients, which stay close to unity as seen in Fig. 2.

Figures 7 and S13 compare RAST predictions for Campaign A, which models the aqueous-phase adsorption of ethanol/water mixtures and represents a much narrower range of total fugacity of 1.8–3.4 $\times 10^4$ Pa and a gas-phase composition of 0.03–0.99. The results are shown for four zeolites of various pore sizes and topologies, including DDR, MFI, BEA, and LTA. The PLD of the four zeolites ranges from 3.55 Å for DDR to 6.04 Å for BEA, while the largest-cavity diameter (LCD) ranges from 6.42 Å for BEA to 11.19 Å for LTA. Under the solution-phase conditions, both IAST and various RAST treatments reproduce ethanol loadings from simulations very well (see Table S2). Similar to the observations for Campaign B, IAST overpredicts the amount of water adsorption, while RAST predictions using Scheme 2 Margules activity coefficients give the best agreement, followed by those using bulk Margules activity coefficients. Fortuitously, both sets of Margules parameters give almost perfect agreement for water in MFI, one of the most studied zeolites, but the Margules equation does not seem to reach similar accuracy for a large number of other zeolites.

D. Structural trends

The Ψ-dependent Margules activity model for adsorbed ethanol/water mixtures was determined for siliceous zeolites with PLD ≥ 4 Å.[17] Figure 8 displays the ζ parameter and activity coefficients for water as a function of PLD and LCD. While results from Scheme 1 reflect the outcome of least-squares fitting to activity coefficients computed at each binary state point, Scheme 2 has to be solved with an upper bound on ζ to avoid the optimizer getting trapped in an attempt to continuously increase ζ. The effect of the Ψ dependence was found to be negligible for $\zeta > 10$ and indistinguishable from ignoring the Ψ dependence for $\zeta > 100$, which was therefore chosen as the threshold. Schemes 1 and 2 give 110 and 68 zeolites with ζ above 10, respectively, while they predict 46 and 62 zeolites with $\zeta < 0.1$. As discussed earlier, even for zeolites with small ζ parameters, the benefits of including the Ψ dependence, at least in conjunction with the Margules activity model, appear minimal, especially in modeling solution-phase ethanol/water adsorption.

The fitted Margules model encodes the non-ideal behavior of adsorbed ethanol/water mixtures. To examine if such behavior is correlated with pore dimensions, Fig. 8(b) plots γ_{H2O} as predicted by Eq. (7) for a few combinations of adsorption potential, Ψ, and adsorbed-phase composition, x_{EtOH}. $\Psi = 12$ and $x_{EtOH} = 0.35$ represent an adsorbed phase with a substantial loading and a predominant fraction of water molecules, a condition typically found at very high pressures. At this state, most zeolites have γ_{H2O} between 1 and 1.5, suggesting slightly unfavorable water/ethanol interactions during mixture adsorption compared to water/water interactions in unary adsorption with a similar loading of water. $\Psi = 3$ and $x_{EtOH} = 0.9$

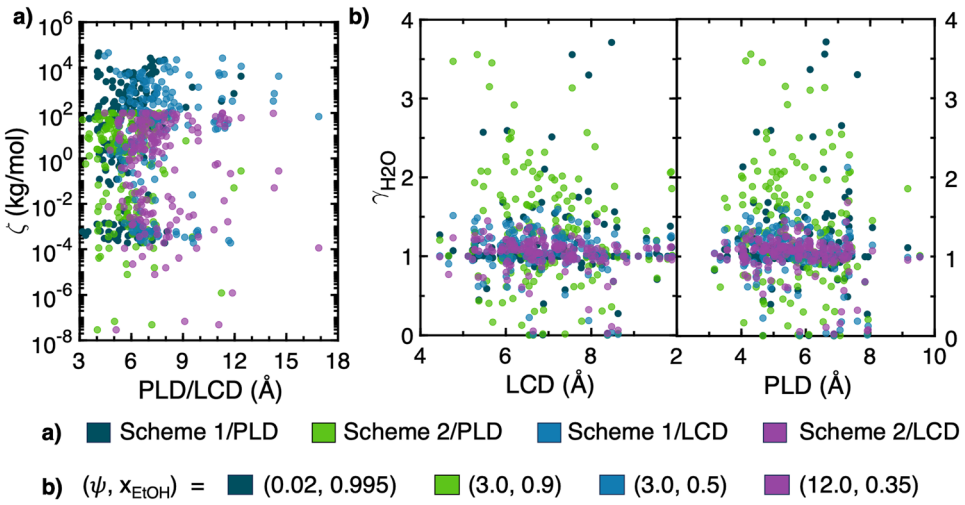

FIG. 8. (a) ζ constants and (b) RAST activity coefficients for water, γ_{H2O}, as a function of pore-limiting diameter (PLD) or largest-cavity diameter (LCD). γ_{H2O} are computed from the fitted Margules equation according to Scheme 2 at different combinations of Ψ and x_{EtOH}.

or 0.5 represent intermediate loadings for zeolites that are more or less selective toward ethanol, while $\Psi = 0.02$ and $x_{EtOH} = 0.995$ represent very small amounts of adsorption of primarily ethanol, typical for the majority of zeolites in the Henry's law regime. Activity coefficients for $\Psi = 3$ and $x_{EtOH} = 0.5$ similarly cluster between 1 and 1.5 with slightly more zeolites exhibiting larger values of γ_{H2O}. On the other hand, when the adsorbed phase consists of primarily ethanol ($x_{EtOH} \geq 0.9$), γ_{H2O} becomes much more scattered, indicating that the effective water/ethanol interactions in dilute adsorbed mixtures is highly modulated by the zeolite structure. However, the dependence of γ_{H2O} on structure is not captured by either PLD or LCD.

IV. CONCLUSIONS

In this work, the adsorption of ethanol/water mixtures in all-silica zeolites was studied using the adsorbed-solution theory of Myers and Prausnitz.[2] GCMC simulations were performed to obtain a comprehensive set of single-component and binary isotherms for all zeolite structures cataloged by IZA with PLD ≥ 4 Å. First, we revisited the high-pressure adsorption from a compressed liquid phase, such as the unary adsorption of water to hydrophobic zeolites. It was found that using appropriate vapor pressure rather than system pressure is critical to a correct IAST/RAST description. Such vapor pressures may not be directly observable in experiments or GEMC simulations but can be computed according to Eq. (12). Using this description, IAST for most zeolites overestimates the loadings of water upon co-adsorption with ethanol, suggesting a positive excess free energy in the adsorbed phase.

Next, RAST analysis was conducted for all zeolites. Even though simulations provide relatively smooth adsorption isotherms, activity coefficients based on RAST can be surprisingly noisy, making it difficult to derive a reliable, unique solution of the activity model. The dependence of activity model on adsorption potential, Ψ, as proposed by Myers[11,18] [e.g., Eq. (7) for the Margules equation], was especially challenging to determine. It was also demonstrated that accurate unary isotherms in the low-loading regime are critical for obtaining physically sensible activity coefficients. In addition, the global regression scheme to solve for activity model parameters (Scheme 2) performs better than fitting activity models to activity coefficients calculated locally (Scheme 1). Overall, the Margules equation struggles to describe the activity coefficients for the ethanol/water system over the entire range of fugacities and compositions examined in this work.

A clear trend of how activity coefficients vary with pore diameters was not identified. In general, the majority of all-silica zeolites were found to be ethanol selective. At low to intermediate total loadings, the adsorbed phase consists of primarily ethanol. The activity coefficients of water under these conditions are highly structure-dependent. On the other hand, at intermediate to high total loadings and higher molar fraction of water, the activity coefficients of water fall between 1 and 1.5, indicating slightly unfavorable water/ethanol interactions compared to water/water interactions with comparable amounts of adsorbed water molecules.

Finally, despite the imperfect description of activity coefficients using the Margules model, RAST predictions of loadings and selectivities were found to be generally good, except for conditions where the loadings for water exceed those for ethanol in ethanol-selective zeolites. These conditions occur only when the total fugacity and the vapor-phase molar fraction of water are both very high, which are unlikely to be realized under most realistic pressures; at $T = 323$ K, a dilute ethanol/water solution needs to be compressed to above 200 MPa for the fugacity of water to reach 10^5 Pa. In many zeolites, using the Margules parameters for bulk ethanol/water mixtures provides an improved description compared to IAST and including Ψ-dependence offers a minor benefit for describing the binary isotherms at the lowest fugacities (e.g., $f_{EtOH} < 10^3$ Pa).

SUPPLEMENTARY MATERIAL

The supplementary material encompasses additional tables, figures, and adsorption isotherms for water, ethanol, and binary ethanol/water mixtures from GCMC simulations for all IZA zeolites with PLD > 4 Å.

ACKNOWLEDGMENTS

This work was supported by the donors of the ACS Petroleum Research Fund under Doctoral New Investigator Grant No. 65230-DNI5 and by the National Science Foundation under Award CBET-2144360 (A.V.L. and P.B.), and by the U.S. Department of Energy, Office of Science, Basic Energy Sciences under Award No. DE-SC0023454, as part of the Computational and Theoretical Chemistry Program (J.I.S.). The calculations used resources of the National Energy Research Scientific Computing Center (NERSC), a Department of Energy Office of Science User Facility using NERSC Award No. ERCAP0028612 and of the Advanced Cyberinfrastructure Coordination Ecosystem: Services & Support (ACCESS) through Allocation No. CTS190069, which is supported by the National Science Foundation under Grant Nos. 2138259, 2138286, 2138307, 2137603, and 2138296.

AUTHOR DECLARATIONS

Conflict of Interest

The authors have no conflicts to disclose.

Author Contributions

Anne V. Le: Investigation (equal); Writing – original draft (equal). **Michael Tsapatsis**: Writing – review & editing (equal). **J. Ilja Siepmann**: Writing – review & editing (equal). **Peng Bai**: Supervision (equal); Writing – review & editing (equal).

DATA AVAILABILITY

The data that support the findings of this study are available within the article and its supplementary material.

REFERENCES

[1] D. M. Ruthven, *Principles of Adsorption and Adsorption Processes* (John Wiley & Sons, New York, 1984).
[2] A. L. Myers and J. M. Prausnitz, "Thermodynamics of mixed-gas adsorption," AIChE J. **11**, 121–127 (1965).
[3] K. S. Walton and D. S. Sholl, "Predicting multicomponent adsorption: 50 years of the ideal adsorbed solution theory," AIChE J. **61**, 2757–2762 (2015).

[4]N. F. Cessford, N. A. Seaton, and T. Düren, "Evaluation of ideal adsorbed solution theory as a tool for the design of metal–organic framework materials," Ind. Eng. Chem. Res. **51**, 4911–4921 (2012).
[5]F. Gharagheizi and D. S. Sholl, "Comprehensive assessment of the accuracy of the ideal adsorbed solution theory for predicting binary adsorption of gas mixtures in porous materials," Ind. Eng. Chem. Res. **61**, 727–739 (2022).
[6]R. Krishna, J. M. van Baten, and R. Baur, "Highlighting the origins and consequences of thermodynamic non-idealities in mixture separations using zeolites and metal-organic frameworks," Microporous Mesoporous Mater. **267**, 274–292 (2018).
[7]R. Krishna and J. M. van Baten, "Water/alcohol mixture adsorption in hydrophobic materials: Enhanced water ingress caused by hydrogen bonding," ACS Omega **5**, 28393–28402 (2020).
[8]R. Krishna and J. M. van Baten, "How reliable is the ideal adsorbed solution theory for the estimation of mixture separation selectivities in microporous crystalline adsorbents?," ACS Omega **6**, 15499–15513 (2021).
[9]R. Krishna and J. M. van Baten, "Fundamental insights into the variety of factors that influence water/alcohol membrane permeation selectivity," J. Membr. Sci. **698**, 122635 (2024).
[10]R. Krishna and J. M. van Baten, "Elucidating the failure of the ideal adsorbed solution theory for CO_2/H_2O mixture adsorption in CALF-20," Sep. Purif. Technol. **352**, 128269 (2025).
[11]F. R. Siperstein and A. L. Myers, "Mixed-gas adsorption," AIChE J. **47**, 1141–1159 (2001).
[12]G. Calleja, A. Jimenez, J. Pau, L. Domínguez, and P. Pérez, "Multicomponent adsorption equilibrium of ethylene, propane, propylene and CO_2 on 13X zeolite," Gas Sep. Purif. **8**, 247–256 (1994).
[13]S. Sochard, N. Fernandes, and J.-M. Reneaume, "Modeling of adsorption isotherm of a binary mixture with real adsorbed solution theory and nonrandom two-liquid model," AIChE J. **56**, 3109–3119 (2010).
[14]H. Kabir, G. Grevillot, and D. Tondeur, "Equilibria and activity coefficients for non-ideal adsorbed mixtures from perturbation chromatography," Chem. Eng. Sci. **53**, 1639–1654 (1998).
[15]G. Gamba, R. Rota, G. Storti, S. Carra, and M. Morbidelli, "Absorbed solution theory models for multicomponent adsorption equilibria," AIChE J. **35**, 959–966 (1989).
[16]N. Mittal, P. Bai, J. I. Siepmann, P. Daoutidis, and M. Tsapatsis, "Bioethanol enrichment using zeolite membranes: Molecular modeling, conceptual process design and techno-economic analysis," J. Membr. Sci. **540**, 464–476 (2017).
[17]C. Baerlocher and L. B. McCusker, Database of zeolite structures, 2013, http://www.iza-structure.org/databases/ (accessed March 2020).
[18]O. Talu, J. Li, and A. L. Myers, "Activity coefficients of adsorbed mixtures," Adsorption **1**, 103–112 (1995).
[19]O. Talu and I. Zwiebel, "Multicomponent adsorption equilibria of nonideal mixtures," AIChE J. **32**, 1263–1276 (1986).
[20]R. T. Yang, *Gas Separation by Adsorption Processes* (Butterworths, Boston, 1987).
[21]P. Bai, M. Tsapatsis, and J. I. Siepmann, "Multicomponent adsorption of alcohols onto silicalite-1 from aqueous solution: Isotherms, structural analysis, and assessment of ideal adsorbed solution theory," Langmuir **28**, 15566–15576 (2012).
[22]J. M. Smith, H. C. Van Ness, M. M. Abbott, and M. T. Swihart, *Introduction to Chemical Engineering Thermodynamics*, 9th ed. (McGraw-Hill Education: New York, 2022).
[23]D. Frenkel and B. Smit, *Understanding Molecular Simulation: From Algorithms to Applications*, 2nd ed. (Academic Press, San Diego, 2001).
[24]T. F. Willems, C. H. Rycroft, M. Kazi, J. C. Meza, and M. Haranczyk, "Algorithms and tools for high-throughput geometry-based analysis of crystalline porous materials," Microporous Mesoporous Mater. **149**, 134–141 (2012).
[25]H. Gies, "Studies on clathrasils. IX: Crystal structure of deca-dodecasil 3R, the missing link between zeolites and clathrasils," Z. Kristallogr. - Cryst. Mater. **175**, 93–104 (1986).
[26]M. Calligaris, G. Nardin, and L. Randaccio, "Cation site location in hydrated chabazites. Crystal structure of potassium- and silver-exchanged chabazites," Zeolites **3**, 205–208 (1983).
[27]J. I. Siepmann and D. Frenkel, "Configurational bias Monte Carlo: A new sampling scheme for flexible chains," Mol. Phys. **75**, 59–70 (1992).
[28]P. Bai and J. I. Siepmann, "Assessment and optimization of configurational-bias Monte Carlo particle swap strategies for simulations of water in the Gibbs ensemble," J. Chem. Theory Comput. **13**, 431–440 (2017).
[29]J. J. de Pablo, M. Laso, J. I. Siepmann, and U. W. Suter, "Continuum-configurational-bias Monte Carlo simulations of long-chain alkanes," Mol. Phys. **80**, 55–63 (1993).
[30]D. Frenkel, G. C. A. M. Mooij, and B. Smit, "Novel scheme to study structural and thermal properties of continuously deformable molecules," J. Phys.: Condens. Matter **4**, 3053–3076 (1992).
[31]W. L. Jorgensen, J. Chandrasekhar, J. D. Madura, R. W. Impey, and M. L. Klein, "Comparison of simple potential functions for simulating liquid water," J. Chem. Phys. **79**, 926–935 (1983).
[32]B. Chen, J. J. Potoff, and J. I. Siepmann, "Monte Carlo calculations for alcohols and their mixtures with alkanes. Transferable potentials for phase equilibria. 5. United-atom description of primary, secondary, and tertiary alcohols," J. Phys. Chem. B **105**, 3093–3104 (2001).
[33]P. Bai, M. Tsapatsis, and J. I. Siepmann, "TraPPE-zeo: Transferable potentials for phase equilibria force field for all-silica zeolites," J. Phys. Chem. C **117**, 24375–24387 (2013).
[34]R. F. DeJaco, M. Dorneles de Mello, H. G. T. Nguyen, M. Y. Jeon, R. D. van Zee, M. Tsapatsis, and J. I. Siepmann, "Vapor- and liquid-phase adsorption of alcohol and water in silicalite-1 synthesized in fluoride media," AIChE J. **66**, e16868 (2020).
[35]P. Bai, M. Y. Jeon, L. Ren, C. Knight, M. W. Deem, M. Tsapatsis, and J. I. Siepmann, "Discovery of optimal zeolites for challenging separations and chemical transformations using predictive materials modeling," Nat. Commun. **6**, 5912 (2015).
[36]B. Xue, D. B. Harwood, J. L. Chen, and J. I. Siepmann, "Monte Carlo simulations of fluid phase equilibria and interfacial properties for water/alkane mixtures: An assessment of nonpolarizable water models and of departures from the Lorentz–Berthelot combining rules," J. Chem. Eng. Data **63**, 4256–4268 (2018).
[37]N. Desbiens, I. Demachy, A. H. Fuchs, H. Kirsch-Rodeschini, M. Soulard, and J. Patarin, "Water condensation in hydrophobic nanopores," Angew. Chem., Int. Ed. **44**, 5310–5313 (2005).
[38]C. H. Wang, P. Bai, J. I. Siepmann, and A. E. Clark, "Deconstructing hydrogen-bond networks in confined nanoporous materials: Implications for alcohol-water separation," J. Phys. Chem. C **118**, 19723–19732 (2014).
[39]J. Kuhn, J. M. Castillo-Sanchez, J. Gascon, S. Calero, D. Dubbeldam, T. J. H. Vlugt, F. Kapteijn, and J. Gross, "Adsorption and diffusion of water, methanol, and ethanol in all-silica DD3R: Experiments and simulation," J. Phys. Chem. C **113**, 14290–14301 (2009).